

Paramagnetic Meissner effect in mesoscopic samples.

V.A. Schweigert [†] and F.M. Peeters [‡]

[†] *Institute of Theoretical and Applied Mechanics, Novosibirsk, Russia,*

[‡] *Departement Natuurkunde, Universiteit Antwerpen (UIA), B-2610 Antwerpen, Belgium*

Electronic mail: peeters@uia.ua.ac.be

(October 31, 2018)

Using the non-linear Ginzburg–Landau (GL) theory, we study the magnetic response of different shaped samples in the field-cooled regime (FC). For high external magnetic fluxes, the conventional diamagnetic response under cooling down can be followed by the paramagnetic Meissner effect (PME). A second-order transition from a giant vortex state to a multi-vortex state, with the same vorticity, occurs at the second critical field which leads to the suppression of PME.

PACS number(s): 74.24.Ha, 74.60.Ec, 73.20.Dx

The Meissner effect is considered the most important characteristic property of superconductivity. When a superconductor is cooled down in the presence of an external magnetic field the field is expelled and it behaves as a diamagnet. However, some samples show a paramagnetic response under cooling. The finding of PME (or Wohleben effect) in high- T_c superconductors [1] initiated the appearance of several models interpreting PME as evidence of non-conventional superconductivity in these materials (e.g. see Ref. [2]). However, numerous observations of PME in conventional macroscopic [3–7] and mesoscopic [8] superconductors indicate the existence of another mechanism, which may be explained with GL theory.

Based on results from axial-symmetric solutions of the GL equations by Fink and Presson [9], Cruz *et al.* [3] proposed that PME in their experiments on $Pb_{99}Tl_{01}$ cylinders is caused by a temperature variation of the superconducting density in a giant vortex state with fixed angular momentum [3]. In such a state, the superconducting current, which shields the magnetic field in the vicinity of the sample boundary (essentially the Meissner effect), changes its direction expelling magnetic field *into* the sample that can lead to the PME. Thereafter this idea, often called *flux compression*, was exploited in [8,10,11], but a quantitative analysis of PME within GL theory is still missing and several principal questions remain to be answered: 1) is the vorticity of the giant vortex state fixed during cooling down as was assumed in Refs. [3,10]? 2) if yes, can this lead to the appearance of PME?, and, finally, 3) can the proposed mechanism explain the PME in recent experiments with conventional macroscopic [3–7] and mesoscopic [8] samples? In this Letter, we follow the GL approach and address these questions by studying the magnetic response of different-shaped samples in the FC regime.

We consider a defect-free superconducting disk (and cylinder) immersed in an insulating media with a perpendicular (along cylinder axis) uniform magnetic field H_0 . The behaviour of the superconductor is characterized by its radius R (and thickness d for the disk case), magnetic field H_0 , the coherence $\xi(T) = \xi(0)(1 - T/T_c)^{-1/2}$ and penetration $\lambda(T) = \lambda(0)(1 - T/T_c)^{-1/2}$ lengths, where T_c is the critical temperature. To reduce the number of independent variables we measure the distance in units of the sample radius, the vector potential \vec{A} in $\hbar/2eR$, and the order parameter Ψ in $\sqrt{-\alpha/\beta}$ with α, β being the GL coefficients [12]. Then the GL equations become

$$\left(-i\vec{\nabla}_{2D} - \vec{A}\right)^2 \Psi = \frac{R^2}{\xi^2} \Psi(1 - |\Psi|^2), \quad (1)$$

$$-\Delta_{3D}\vec{A} = \frac{R^2}{\lambda^2} f(z) \vec{j}_{2D}. \quad (2)$$

Here, the indices $2D$, $3D$ refer to two-dimensional and three-dimensional operators;

$$\vec{j}_{2D} = \frac{1}{2i} \left(\Psi^* \vec{\nabla}_{2D} \Psi - \Psi \vec{\nabla}_{2D} \Psi^* \right) - |\Psi|^2 \vec{A}, \quad (3)$$

is the density of superconducting current in the plane (x, y) , and the external magnetic field is directed along the z -axis. The boundary conditions to Eqs. (1-2) correspond to zero superconducting current at the sample boundary and uniform magnetic field far from the sample. The order parameter and superconducting current are assumed to be independent of the z -coordinate which is valid for cylinders as well as for thin $d \ll \xi, \lambda$ disks [13–15]. Then $f(z) = 1$ and $f(z) = d\delta(z)$ for the cylindrical and disk geometry, respectively.

Superconducting disks and cylinders placed in a magnetic field and cooled down transit from a normal to a superconducting state at the critical temperature T_* , which depends both on H_0 and R . However, the unitless parameters $H_0/H_{c2}(T_*)$, $R/\xi(T_*)$, and the angular momentum of the giant vortex superconducting state in the nucleation point T_* depend only on the magnetic flux $\Phi = \pi R^2 H_0$ piercing through the sample [14]. Here, $H_{c2} = \Phi_0/2\pi\xi^2$ and $\Phi_0 = hc/2e$ are the second critical field and the flux quantum, respectively. With further cooling down, the magnetic response is characterized by only two independent variables H_0/H_{c2} and Φ .

Our numerical approach for solving Eqs. (1-2) is described in [13–15]. It turns out that an accurate simulation of a multi-vortex state is a hard task in the case

of large vorticity L . The latter corresponds to the total angular momentum and the number of vortices in the giant-vortex and the multi-vortex state, respectively. To improve the accuracy we apply a non-uniform rectangular space grid condensing in the vicinity of the sample boundary. However, due to the tremendous computational expenses (e.g. the total number of grid points in the plane (x, y) was about 160000 for $L = 30$) we could only treat the vortex state with large L in the cylindrical case, when the vector potential is uniform in the z -direction. In the disk case, we restrict our considerations to the axial symmetric solutions $\Psi = \psi(\rho)\exp(iL\phi)$ (ρ, ϕ are the cylindrical coordinates), which are shown to be stable in the region $H_0 > H_{c2}$.

When the sample is cooled down below the critical temperature T_* , a giant vortex state appears with angular momentum L , which is determined by the magnetic flux Φ [10,14,16]. Starting from this state we mimic the FC regime by decreasing (increasing) slowly the value of $H_0/H_{c2} \sim 1/(1 - T/T_c)$ ($R^2/\xi^2 \sim (1 - T/T_c)$) such that the system evolves along a path with fixed external magnetic flux (e.g. see Fig. 1). Using the superconducting state found at the previous step as input, we find the next steady-state solution to Eqs. (1-2). Doing so we consider only stable solutions and neglect thermal fluctuations, which could lead to possible transitions between metastable states. This assumption is valid for normal superconductors where the barriers separating the metastable states exceed by far the sample temperature, except near points in which the state becomes unstable [17], e.g. near the saddle points.

When calculating the dipole magnetic moment, we can neglect non-linear effects in the vicinity of the nucleation point. The quantum angular momentum L increases almost proportional to the magnetic flux Φ but remains always smaller than Φ/Φ_0 . The supervelocity $v_\phi = \rho^{-1}(L - \Phi\rho^2/\Phi_0 R^2)$, which is oriented along the azimuthal direction, changes its sign at $\rho_* = R\sqrt{L\Phi_0/\Phi}$. Therefore, both diamagnetic ($\rho > \rho_*$) and paramagnetic ($\rho < \rho_*$) currents exist in any giant vortex state. However, the magnetic moment, which can be estimated in the lowest Landau level (LLL) approximation as $D \sim \int d\rho \rho^2 v_\phi |\psi_L|^2$ with ψ_L being the lowest eigenfunction of the linearized first GL equation, turns out to be always diamagnetic both for disks and cylinders. As long as the superconducting density $|\Psi|^2$ remains small, the magnetic moment almost linearly increases in absolute value with decreasing H_0/H_{c2} (inset (a) in Fig. 1). With further cooling down, the LLL approximation breaks down. Due to non-linear effects (mainly from the second term in the RHS of Eq. (1)) the order parameter increases more rapidly in the inner region which leads to an increase of the paramagnetic component (Figs. 1,2).

The resulting magnetic moment crucially depends on the ratio between L and Φ/Φ_0 . With increasing magnetic field, the switching $L \rightarrow L + 1$ of the angular momentum of the nucleated state occurs at a certain Φ_L [14]. For

given L , the magnetic moment reaches its maximum and minimum value at Φ_{L-1} and Φ_L , respectively. Due to angular momentum quantization the magnetic moment exhibits a strong oscillating behaviour as function of the magnetic field (see inset of Fig. 3) which agrees with Geim's observations [8]. With decreasing temperature, the dipole magnetic moment becomes zero for certain ratio $H/H_{c2} \sim 1/(1 - T/T_c)$ and the original diamagnetic response becomes paramagnetic. This magnetic field is shown in Fig. 3 for $\Phi = \Phi_{L-1}$ and $\Phi = \Phi_L$. Note that: 1) for the cylinder geometry a larger GL parameter $\kappa = \lambda/\xi$ favours PME, 2) while an increase of the effective penetration length λ^2/d suppresses PME in disks, and 3) an increase of Φ favours PME both in cylinders and disks. The reason is that the point ρ_* , where the supervelocity changes its direction, shifts towards the sample boundary with increasing angular momentum which is related to the total magnetic flux $\Phi(L \gg 1) \approx \Phi_0(L + L^{1/2})$ [16].

In cylinders, the magnetization is directly proportional to the magnetic moment. In disks: 1) the diamagnetic currents flowing near the sample boundary give larger contributions to the magnetization than inner paramagnetic currents [11] and consequently, the paramagnetic contribution to the magnetization will be strongly suppressed (inset (b) in Fig. 1), 2) but the smaller trapped magnetic flux, in disks as compared to cylinders, decreases the diamagnetic response. This is the reason why thicker disks show onset of PME at larger H_0/H_{c2} (Fig. 3, open symbols).

When the second critical field $H_{c2}(T)$ becomes smaller than the applied magnetic field, the giant-vortex state transits to the multi-vortex state with the same vorticity (Figs. 4,5). This *second-order transition* is not followed by any jumps in the magnetization or the magnetic moment. Just after the transition, all vortices are arranged in a ring (0:L). Note, that the magnetic moment of the state (0:L) continues to increase with decreasing $H_0/H_{c2}(T)$ but with a smaller slope (Fig. 5). With further decreasing $H_0/H_{c2}(T)$ a pair of vortices moves to the inner region and the state (2:L-2) appears for $L = 20$ (see Fig. 5). This *first-order transition* is followed by a weak jump in the magnetic moment. The derivative dD/dT changes sign and further cooling down results in the disappearance of PME. The magnetic moment of the diamagnetic state with smaller angular momentum $L = 19$ and $\Phi = \Phi_L$ is also affected by the transition to the multi-vortex state, which increases the diamagnetic response (inset (b) in Fig. 4). As the temperature decreases, vortices continue to move from the outer to the inner shell. Note, that the corresponding weak jumps in the magnetic moment are practically not visible on the scale used in Fig. 4. Although the state with $L = 19$ is energetically more favourable than the one with $L = 20$, no vortex exits the system which is in agreement with observations [8]. Since the vorticity remains unchanged under cooling down, the magnetic response will be almost reversible. The hysteresis caused by the first-order transitions between different multi-vortex states with the

same vorticity is weak (see inset (a) of Fig. 4). Starting from the point $H/H_{c2} = 0.9$ and warming up the system to $H/H_{c2} = 1.1$ we find the magnetic moment, which coincides in the scale of Fig. 4 with that obtained by cooling down.

Although the magnetization curves, shown in Fig. 4, agree qualitatively with those from experiments [4–6], a number of issues remain unclear: 1) in experimental observations of macroscopic samples a weak hysteresis is found in cooling down and subsequent warming up, and 2) the observed maximum in the magnetic momentum are weaker than those from our calculations which may be due to the presence of vortex pinning centra. Note that within GL theory we found a weak PME which is caused by the competition of large diamagnetic and paramagnetic responses of the outer and inner part of the sample, respectively. Any mechanism which slightly influences any of the two responses may strongly influence the total magnetic behavior. As an example, in macroscopic disks PME disappears after mechanical abrading the top and bottom surfaces [4–6]. A number of samples made from the same material as those demonstrating PME exhibited only diamagnetic behaviour [4–6]. This indicates the important role played by the sample structural inhomogeneity. For mesoscopic disks, experiments [8] show PME for rather small angular momenta which does not agree with our simulations for flat circular mesoscopic disks.

To address some of these sample structural issues we consider the influence of the superconductor shape on the magnetic moment by varying radially the thickness of the disk. We limit ourselves to the case of a strong type-II superconductor ($\kappa \gg 1$) and solve, therefore, only Eq. (1). The dipole magnetic moment of different-shaped samples is shown in Fig. (6) for $H_0 = H_{c2}(T)$, where the scale of the thickness variation is apparent from the insets of Fig. 6. The magnetic moment becomes more negative (positive) in magnifying glass (crown) like samples as compared to flat disks. An increase of the local thickness near the sample boundary (see Fig. 6(c)) increases the PME. This strongly suggests a possible non flat geometry of the disks of Ref. [8].

In summary, the giant-vortex state remains stable under cooling down and transits to the multi-vortex state with the same vorticity at $H_0 \approx H_{c2}$. The paramagnetic response is caused by a more rapid growth of the superconducting electron density in the inner region of the sample, due to non-linear effects, where paramagnetic currents flow. The appearance of the multi-vortex state suppresses PME and the maximum of the paramagnetic response corresponds to $H_0 \approx H_{c2}$. We showed that within the GL theory a paramagnetic response is possible for large magnetic fluxes, which is in agreement with experimental findings on disks with large radii, but does not agree with the experimental results on mesoscopic disks of Geim *et al* [8].

After finishing this work, we came aware of a preprint by Palacios [18] who used the LLL approximation to

study the FC regime and failed to find any paramagnetic response. As shown above, one has to go beyond the LLL approximation in order to find PME which is caused by non-linear effects.

We thank A.K. Geim for useful discussions. This work is supported by the Flemish Science Foundation (FWO-VI) and the “Interuniversity Poles of Attraction Program - Belgian State, Prime Minister’s Office - Federal Office for Scientific, Technical and Cultural Affairs”. One of us (VAS) was supported by a DWTC fellowship and (FMP) is a research director with the FWO-VI.

-
- [1] W. Braunisch, N. Knauf, V. Kataev, S. Neuhausen, A. Grütz, A. Kock, D. Khomskii, and D. Wohlleben, *Phys. Rev. Lett.* **68**, 1908 (1992).
 - [2] M. Sigrist and T.M. Rice, *J. Phys. Soc. Jpn.* **61**, 4283 (1992).
 - [3] F. de la Cruz, H.J. Fink, and J. Luzuriaga, *Phys. Rev. B* **20**, 1947 (1979).
 - [4] D.H. Thompson, M.S.M. Minhaj, L.E. Wenger, and J.T. Chen, *Phys. Rev. Lett.* **75**, 529 (1995).
 - [5] P. Kostic, B. Veal, P. Paulikas, U. Welp, V.R. Todt, C. Gu, U. Geiser, J.W. Williams, K.D. Carlson, and R.A. Klemm, *Phys. Rev. B* **53**, 791 (1996).
 - [6] L. Pust, L.E. Wenger, and M.R. Koblischka, *Phys. Rev. B* **58**, 14191 (1998).
 - [7] A. Terentiev, D.B. Watkins, L.E. De Long, D.J. Morgan, and J.B. Ketterson, *Phys. Rev. B* **60**, R761 (1999).
 - [8] A.K. Geim, S.V. Dubonos, J.G.S. Lok, M. Henini, and J.C. Maan, *Nature (London)* **396**, 144 (1998).
 - [9] H.J. Fink and A.G. Presson, *Phys. Rev.* **151**, 219 (1966).
 - [10] V.V. Moshchalkov, X.G. Qiu, and V. Bruyndoncx, *Phys. Rev. B* **56**, 11793 (1997).
 - [11] A.E. Koshelev and A.I. Larkin, *Phys. Rev. B* **52**, 13559 (1995).
 - [12] P.G. de Gennes, *Superconductivity of metals and alloys*, (Addison-Wesley, N.Y., 1989).
 - [13] P.S. Deo, V.A. Schweigert, F.M. Peeters, and A.K. Geim, *Phys. Rev. Lett.* **79**, 4653 (1997).
 - [14] V.A. Schweigert and F.M. Peeters, *Phys. Rev. B* **57**, 13817 (1998).
 - [15] V.A. Schweigert, F.M. Peeters, and P.S. Deo, *Phys. Rev. Lett.* **81**, 2783 (1998).
 - [16] R. Benoist and W. Zwerger, *Z. Phys. B* **103**, 377 (1997).
 - [17] V.A. Schweigert and F.M. Peeters, *Phys. Rev. Lett.* **83**, 2409 (1999).
 - [18] J.J. Palacios, cond-mat/9908341.

FIG. 1. The nucleation field as a function of the radius. Thin curves show the path along which the system evolves during cooling down. Insets (a) and (b) show the corresponding dipole magnetic moment and magnetization ($M = H_{c2}^{-1} \int d\vec{r} (H_z - H_0)/d\vec{r}$, where integration is performed over the sample volume), respectively. Here, solid and dotted curves correspond to cylinder ($\kappa = 10$) and disk ($\kappa = 1$, $d = 0.1R$), respectively.

FIG. 2. The distribution of the superconducting electrons density (a), the superconducting current (inset) and the magnetic field (b) in the cylinder (solid and dashed curves) and the disk (inset) for different reduced magnetic fields H/H_{c2} : 1-1.6, 2-1.3, 3-1.0.

FIG. 3. The magnetic field corresponding to the transition from the diamagnetic to paramagnetic response as a function of the total angular momentum for $\Phi = \Phi_{L-1}$ and $\Phi = \Phi_L$. Solid and open symbols correspond to cylinders and disks, respectively. Inset shows the magnetic moment of the cylindrical sample at $H_0 = H_{c2}$ and $\kappa = 10$.

FIG. 4. The dipole magnetic moment of cylindrical samples for different external magnetic fluxes $\Phi = \Phi_{L-1}$ and $\kappa = 10$. The hysteretic behaviour is demonstrated in inset (a) for $L = 20$ and $\Phi = \Phi_{L-1}$. Inset (b) shows the magnetic response for $L = 19$ and Φ_L .

FIG. 5. The dipole magnetic moment and contour plots of the superconducting density (log-scale is used) in the vicinity of the second critical field.

FIG. 6. The dipole magnetic moment of different shaped circular samples at $H_0/H_{c2} = 1$.

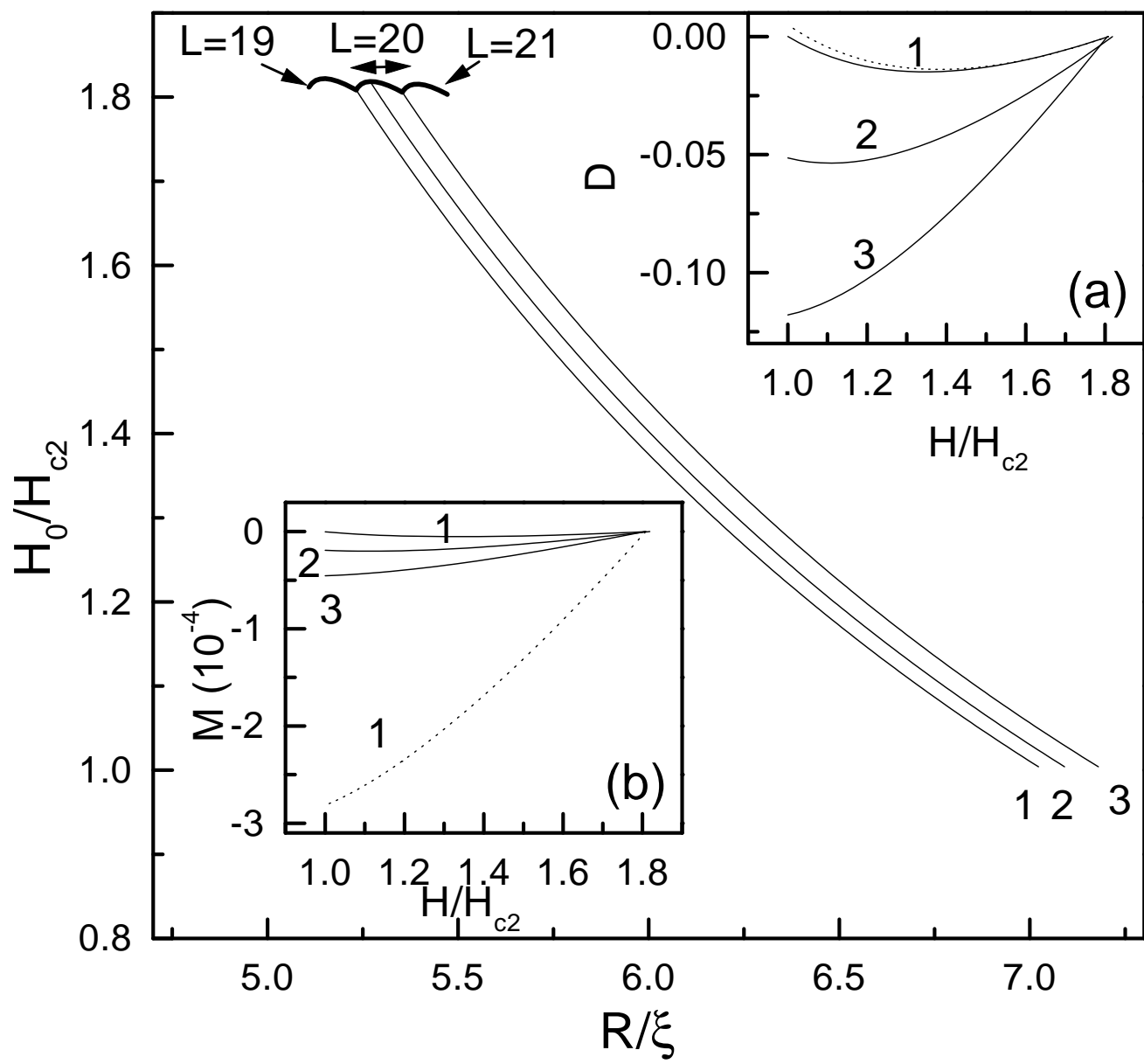


Fig.1

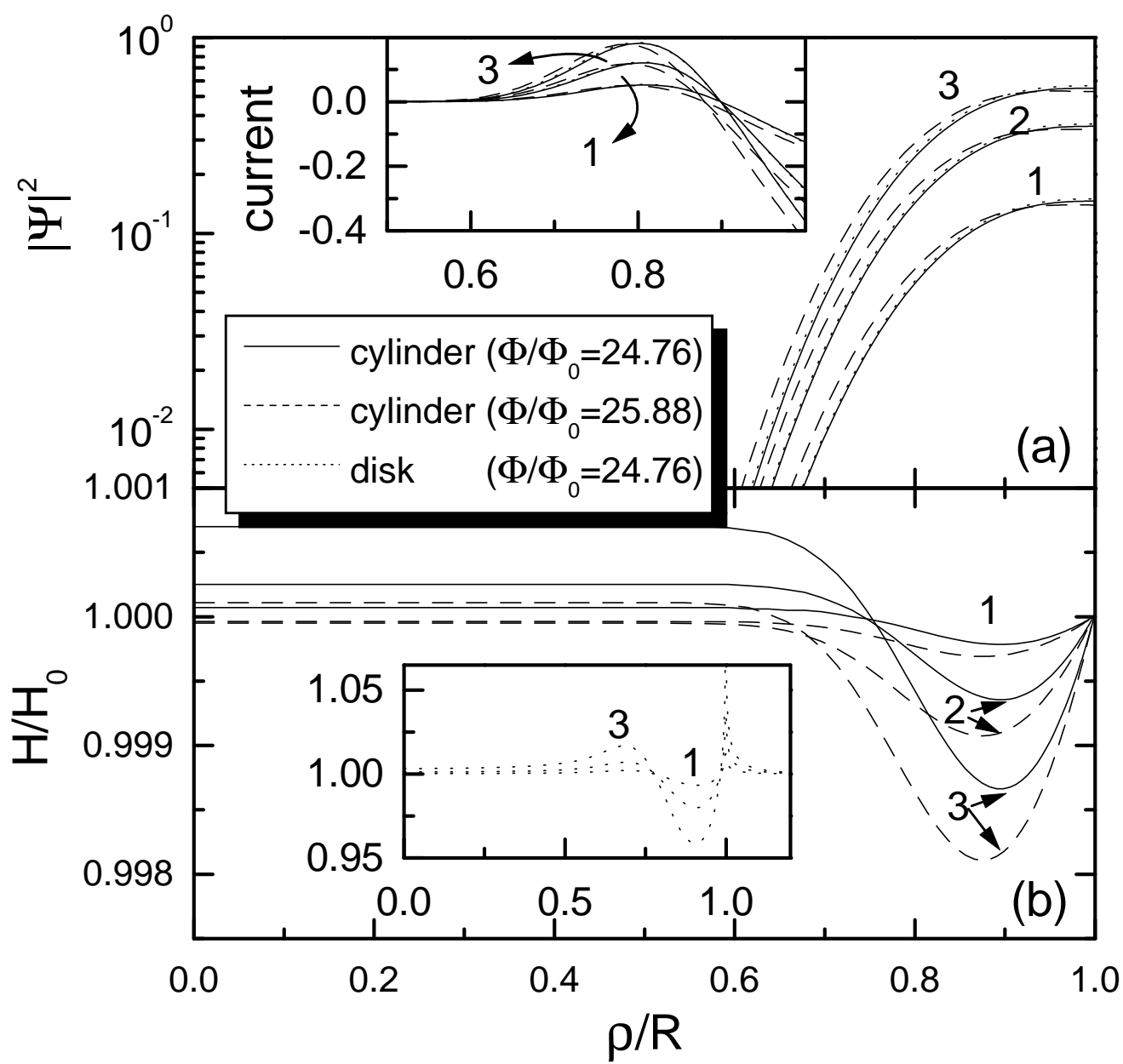


Fig.2

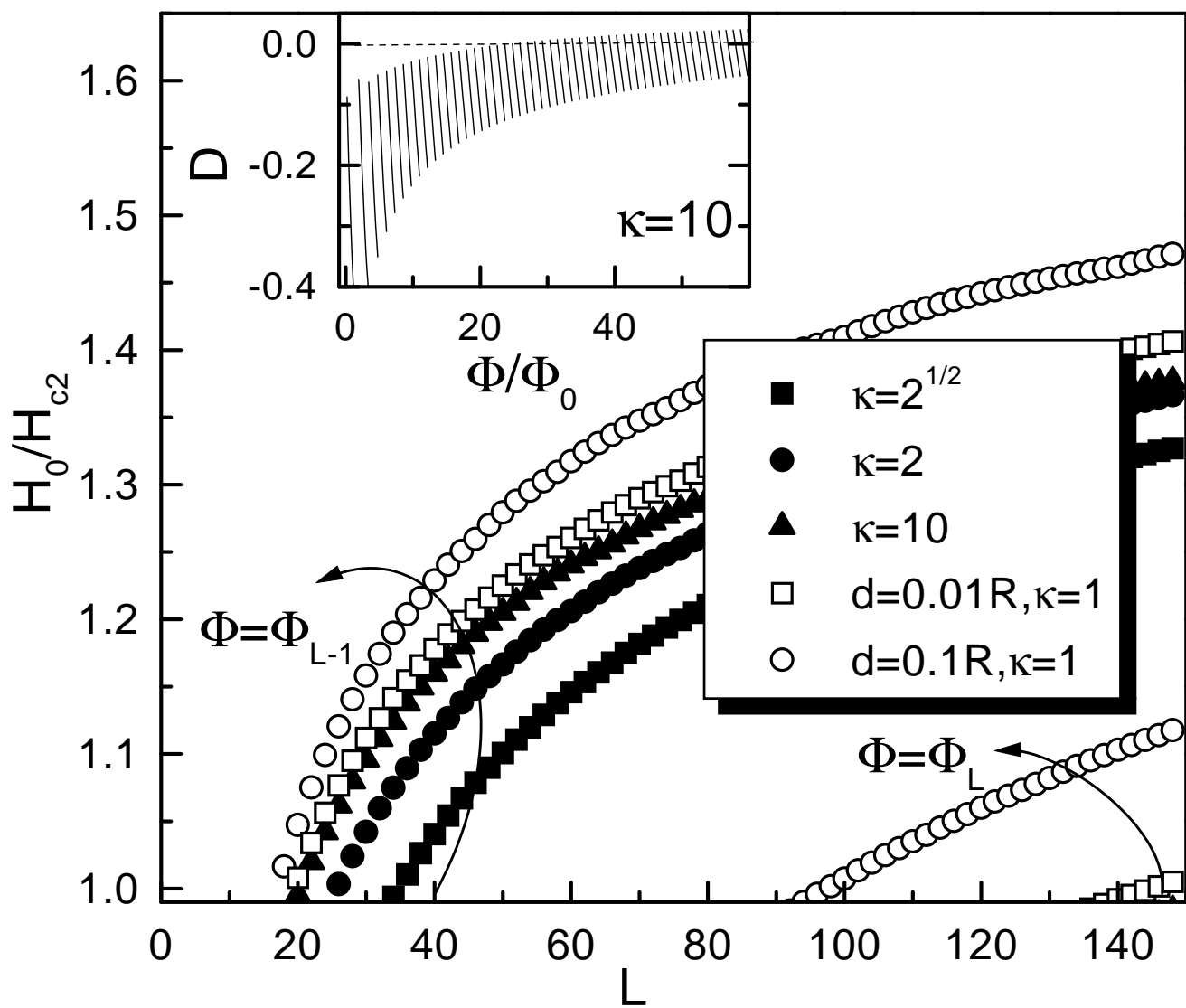


Fig.3

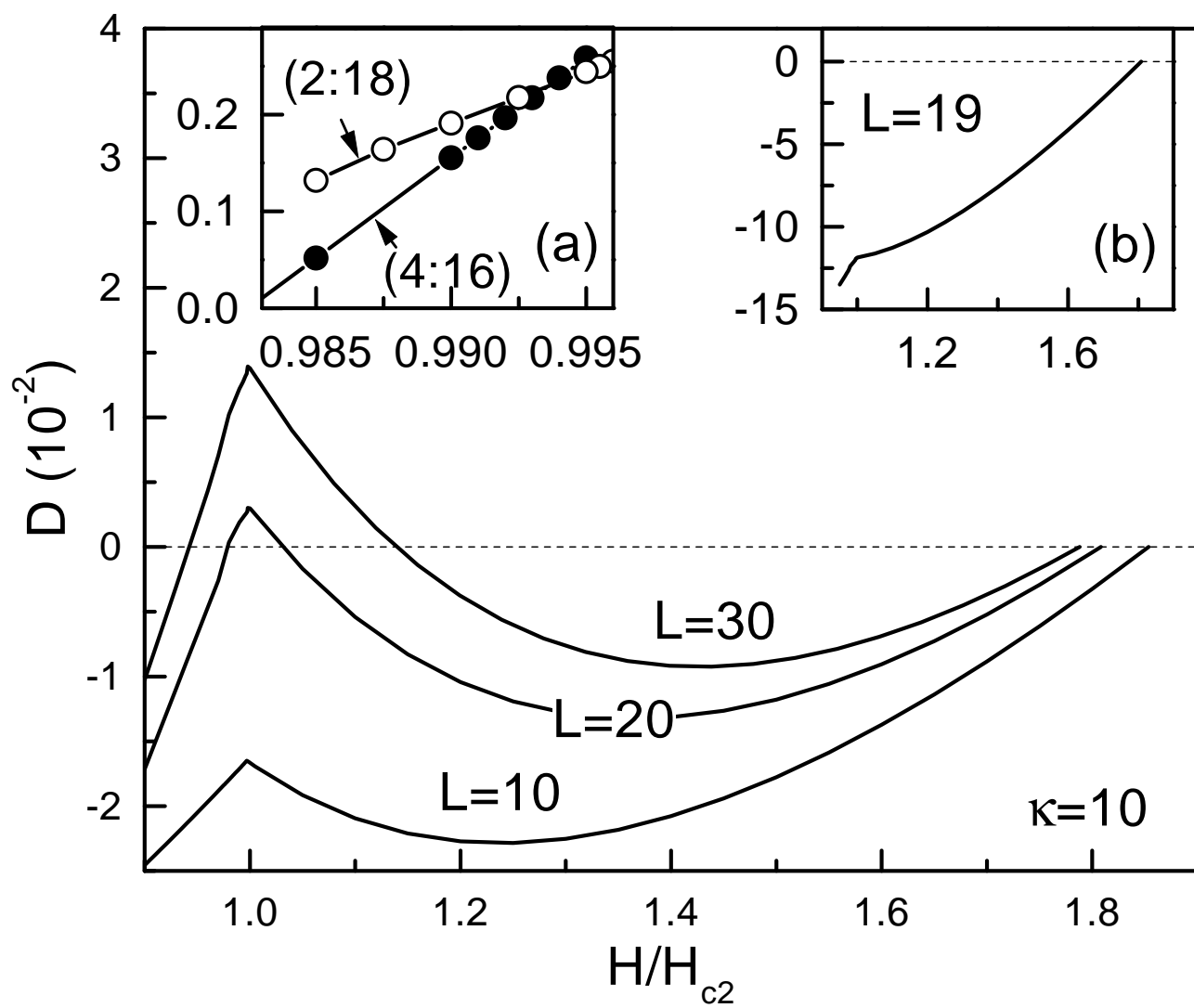


Fig.4

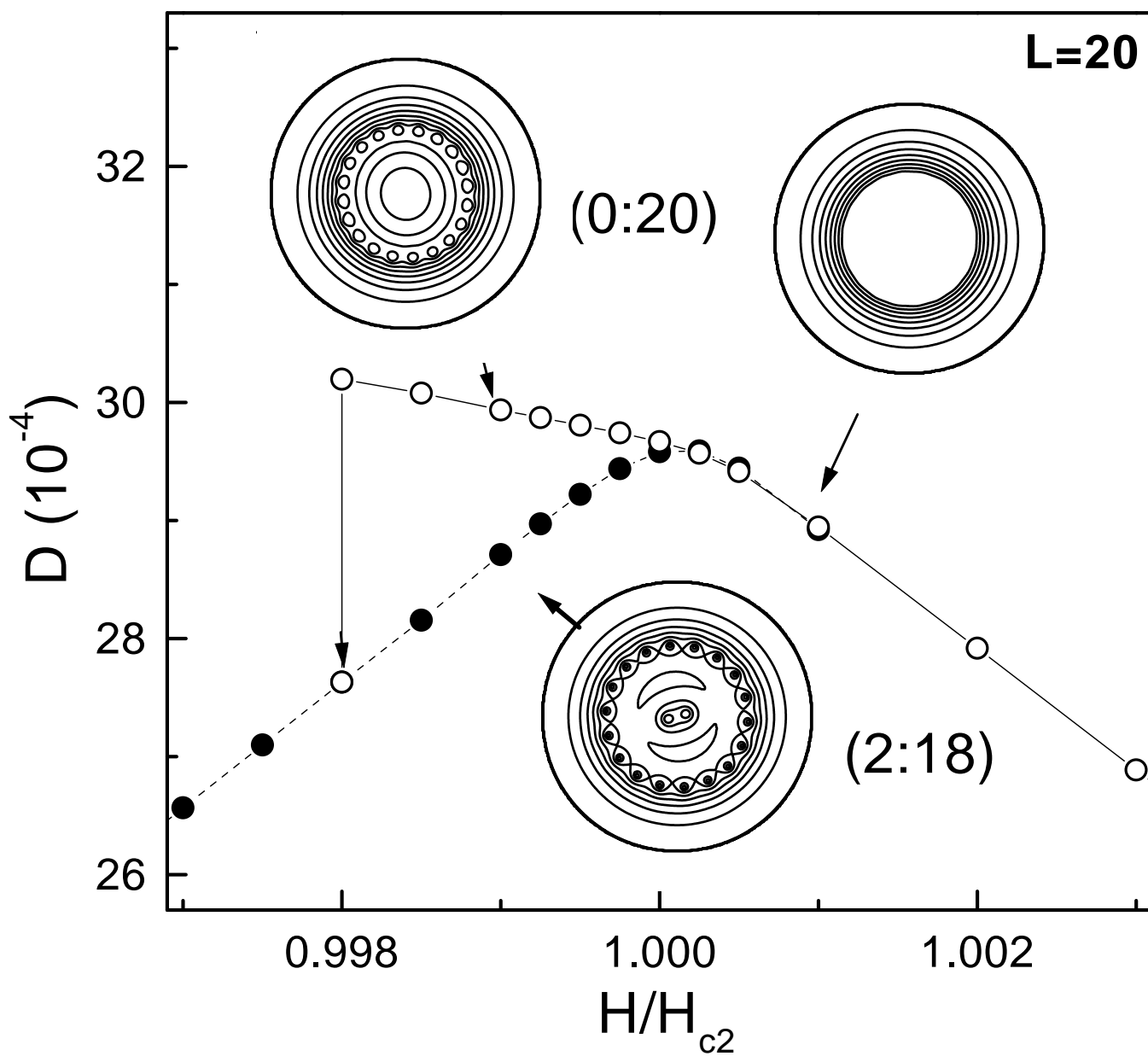


Fig.5

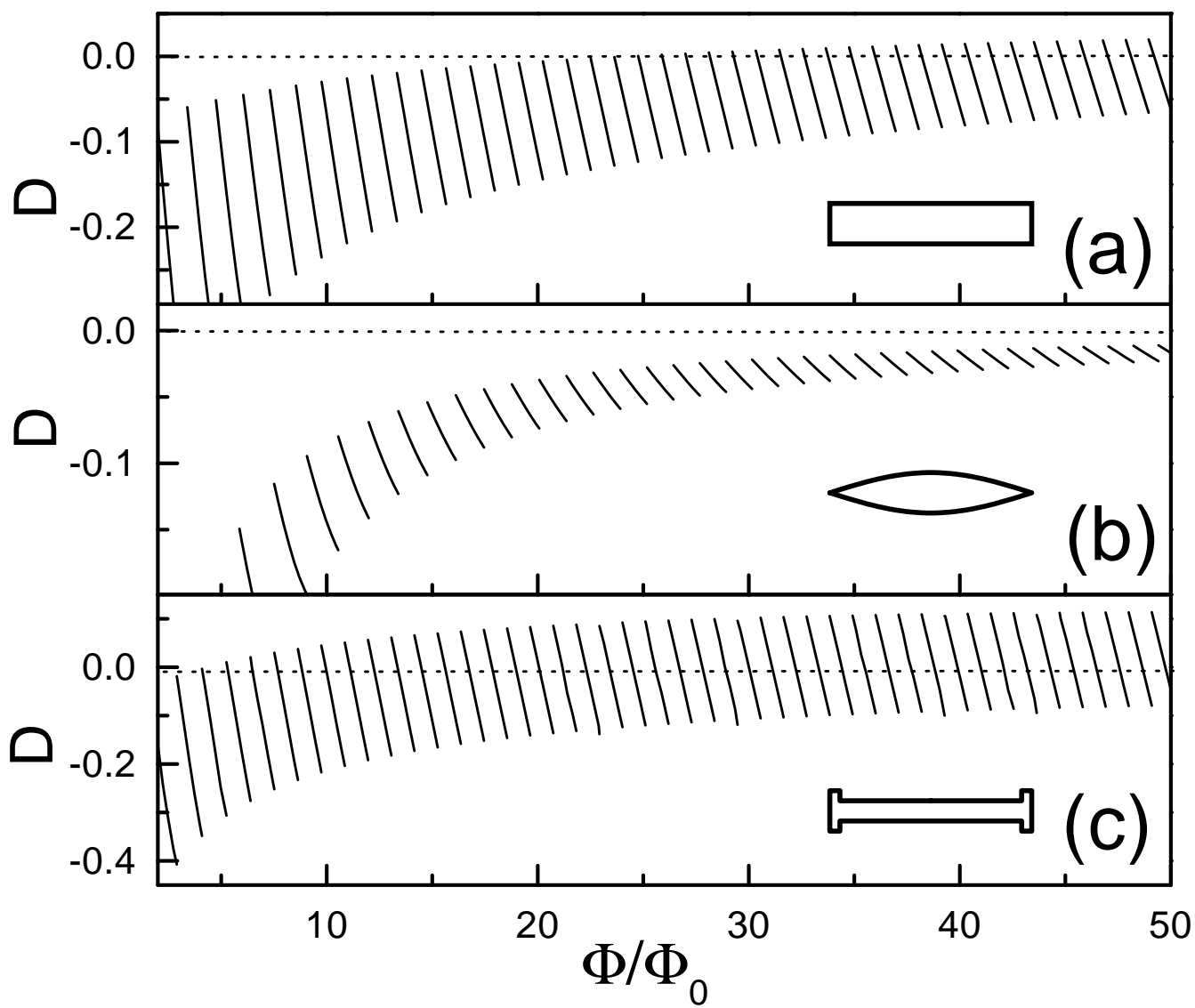


Fig.6